Louisiana State University
LSU Scholarly Repository

Honors Theses | Ogden Honors College

11-2020

Ribosomal RNA synthesis after induced nucleolar stress in Drosophila melanogaster

Kyle Maher

Follow this and additional works at: https://repository.lsu.edu/honors_etd

 Part of the Biology Commons

Recommended Citation

Maher, Kyle, "Ribosomal RNA synthesis after induced nucleolar stress in Drosophila melanogaster" (2020). *Honors Theses*. 967.
https://repository.lsu.edu/honors_etd/967

This Thesis is brought to you for free and open access by the Ogden Honors College at LSU Scholarly Repository. It has been accepted for inclusion in Honors Theses by an authorized administrator of LSU Scholarly Repository. For more information, please contact ir@lsu.edu.

Ribosomal RNA synthesis after induced nucleolar stress in *Drosophila melanogaster*

by Kyle Maher

Undergraduate honors thesis under the direction of

Dr. Patrick J. DiMario

Department of Biological Sciences

Submitted to the LSU Roger Hadfield Ogden Honors College in partial fulfillment of the Upper Division Honors Program.

November 2020

Louisiana State University
& Agricultural and Mechanical College
Baton Rouge, Louisiana

Acknowledgments

I would like to thank my thesis director, Dr. Patrick DiMario, for welcoming me to his lab, continuously educating me, and guiding me throughout this project. I truly appreciate his patience and perseverance with this project as well as his dedication to bolstering my knowledge of science and helping me develop my research skills.

Abstract

The term ribosomopathies defines a group of disorders characterized by a disturbance in the ribosome biogenesis process. A protein known as Nopp140 in particular is thought to be critically involved in several parts of the ribosome biogenesis process. This protein resembles the treacle protein found in humans, which when lost, causes a ribosomopathy known as Treacher Collins Syndrome (TCS). This study investigated how the loss of the *Nopp140* gene in *Drosophila melanogaster,* the common fruit fly, affects the process of rRNA synthesis as a model for TCS in humans.

To observe rRNA synthesis, this study applied the method of BrUTP labeling, which tags newly transcribed RNA *in vivo*. In order to focus on rRNA specifically, the nucleolus was the target of this study, and transcripts within the nucleoli were visualized using indirect immunofluorescence. With the fluorescence microscopy images, ImageJ software was used to calculate the brightness of individual nucleoli as a proxy for rRNA synthesis quantification. While this brightness value for *Nopp140-/+* larvae was higher than *Nopp140-/-* larvae, the values did not seem statistically significant and will thus, require further investigation. Future studies may also help elucidate the effects of the loss of Nopp140 on rRNA synthesis and ribosome production.

Introduction

Ribosomopathies:

Ribosome biogenesis is a complex process orchestrating many moving parts, so disruption along any point in its course – from transcription to assembly – can result in a multitude of consequences. A disturbance of the nucleolus that causes failure of ribosome biogenesis or causes the creation of dysfunctional ribosomes is termed "nucleolar stress" and is responsible for a group of genetic disorders collectively known as ribosomopathies (Narla & Ebert, 2010). Since disruption of the biogenesis process can occur at any point, ribosomopathies can significantly differ in mechanism and clinical presentation and thus, potential for treatment must be specifically tailored for each disorder (Nakhoul et al., 2014).

Notably, all ribosomopathies affect stem cells or progenitor cells (for example, the Treacher Collins Syndrome in humans is a ribosomopathy that affects neural crest cells), yet each ribosomopathy presents a unique phenotype and often displays tissue specificity (Baral et al., 2020). This study proposes *Drosophila melanogaster* as a model for human ribosomopathies by investigating nucleolar stress in larval stage neuroblasts (NBs). Specifically, this study focuses on the production of rRNA in nucleolar stress-induced larvae.

Nucleolus:

In general, ribosome biogenesis requires a lot of energy from the cell (Baral et al., 2020). As part of a natural process, all cells will respond to stress or disruption of their homeostasis by downregulating ribosome biogenesis as a way to preserve cellular energy, and the nucleolus seems to be the control center in charge of responding to such cellular stress (Grummt, 2013).

The nucleolus is a sub-compartment of the nucleus and comprises three compartments itself: the fibrillary centers (FC), dense fibrillary centers (DFC), and granular component (GC) (Grummt, 2013). Notably, the nucleolus is the site of rRNA synthesis (Cooper, 2000). Transcription and processing occur in the DFC, and pre-ribosome assembly occurs in the GC (Grummt, 2013).

Because the nucleolus controls such cardinal functions of ribosome assembly and processing, it is the target of this study. Looking at nucleolar rRNA can give insight into the ribosome production complications seen with ribosomopathies.

Nopp140:

Nucleolar phosphoprotein 140, or Nopp140, is a ribosome assembly factor – also referred to as a ribosome biogenesis factor (RBF) – that serves many purported functions in the ribosome assembly process (Baral et al., 2020). Nopp140 can be found mostly in the DFC of the nucleoli but also in nuclear regions called Cajal bodies, and it seems that Nopp140 shuttles between the nucleoli/nucleus and the cytoplasm (Cui & DiMario, 2007).

The phosphoprotein is known to associate with snoRNPs – both C/D box snoRNPs and H/ACA snoRNPs, which assist in methylation and pseudo-uridylation of pre-RNA, respectively (Cui & DiMario, 2007). It is likely that Nopp140 functions as an assembly factor for these snoRNPs or helps chaperone the snoRNPs between Cajal bodies and the nucleolus (Cui & DiMario, 2007). Nopp140 is also known to interact with RNA Pol I in the nucleolus for regulation of rRNA transcription and with RNA Pol II transcription factors (Cui & DiMario, 2007). Because of this close link to nucleolar ribosome production, the loss of the *Nopp140* gene is predicted to

affect rRNA production and thus, impair ribosome production. The functions of Nopp140 have been inferred by its interactions and localizations with other nucleolar/nuclear components, but its precise function is still being studied.

In *Drosophila melanogaster* specifically, the *Nopp140* gene is positioned in the proximal left arm of the third chromosome (Cui & DiMario 2007). In a 2007 study, Cui and DiMario expressed RNAi using the GAL4/UAS system in *Drosophila* in order to determine the functional significance of Nopp140. Using this method, the *Nopp140* mRNA was successfully depleted to various extents; the resulting flies displayed *Minute*-like phenotype, which presents several characteristic features reminiscent of TCS in humans (Cui & DiMario, 2007). A comprehensive list of features of the *Minute*-like phenotype include short and thin thoracic bristles, missing/deformed antennae, abnormal wings, rough eyes, defective abdominal cuticle segmentation, reduced fertility, prolonged development, reduced viability, and recessive lethality (Cui & DiMario 2007).

A study conducted by Baral et al. (2020) later successfully used CRISPR to disrupt the *Nopp140* gene. In general, larvae homozygous for the *Nopp140* gene disruption are significantly smaller in size compared to the heterozygotes and the wild-type. The larvae homozygous for the *Nopp140* gene disruption also exhibit high embryonic lethality (Baral et al., 2020). Specifically, this study by Baral et al. (2020) found that ~50% of the knockout larvae died just 6 days after hatching. Even the larvae heterozygous for the disruption showed partial lethality (Baral et al., 2020).

Nucleolar stress from the loss of Nopp140 – either by CRISPR-mediated gene disruption or RNAi depletion – also causes impairment in the larval brain development (Baral et al., 2020).

The 2020 study by Baral et al. found that the brains of the early larval stage *Nopp140-/-* larvae were comparable in size to the wild type brains. In the study, homozygous knockout brains continued to grow but at a reduced rate compared to the wild type, and at about 5-6 days after larval hatching (ALH), the mutant brains failed to grow anymore (Baral et al., 2020). In general, the resulting phenotype upon nucleolar stress was brain hypoplasia (Fig. 1), but different NB lineages displayed a variety of phenotypes, ranging from mild-severe loss of the lineage progeny cells to complete loss of the lineage (Baral et al., 2020).

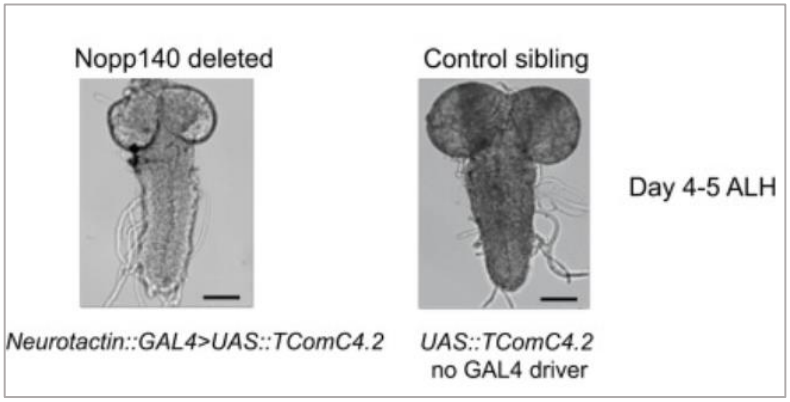

Figure 1. Brain hypoplasia in Nopp140 depleted larvae. Larvae that undergo nucleolar stress, specifically loss of the *Nopp140* gene, display significantly impaired brain development compared to wild type larvae. These images were both taken 4-5 days after larval hatching (ALH).

Treacher Collins Syndrome:

Ribosomopathies tend to present distinct phenotypes, such as the craniofacial abnormalities characteristic of Treacher Collins Syndrome (TCS) in humans (Baral et al., 2020). Specifically, phenotypic markers of TCS include malar and maxillary hypoplasia, slanting palpebral fissures, and malformed ears (Narla & Ebert, 2010). Furthermore, malformation of facial bones may lead to further complications with speech, swallowing, hearing, or brain development (Narla & Ebert, 2010).

The cause of TCS begins in the neural crest cells (Baral et al., 2020). During the process of embryogenesis, a subset of neural crest cells that would normally migrate to pharyngeal arches I and II becomes deficient in functional ribosomes in individuals with TCS (Baral et al., 2020). As a result, p53-dependent apoptosis leads to the loss of these neural crest cells, which subsequently causes the craniofacial defects that are characteristic of TCS (Baral et al., 2020). In other words, the deformities result from a lack of production and/or function of ribosomes within the progenitor neural crest cells (Cui & DiMario 2007).

TCS is specifically caused by a haplo-insufficiency mutation of the *TCOF1* gene that codes for treacle, which is most strongly expressed in the neural crest cells (Baral et al., 2020, Nakhoul et al., 2014). As mentioned, there was partial lethality observed by both homozygous and most notably, heterozygous larvae for the disrupted *Nopp140* gene (Baral et al., 2020). This means that the *Nopp140-/+* genotype also exhibits haplo-insufficiency – similar to the *Tcof1-/+* genotype in humans with TCS (Baral et al., 2020).

In fact, the *Drosophila Nopp140* gene is the closest to the *TCOF1* gene in humans, and the treacle protein product is a nucleolar ribosome biogenesis factor similar to Nopp140 in both structure and function (Baral et al., 2020). Structurally, treacle and Nopp140 orthologues are both comprised of alternating basic and acidic motifs (Baral et al., 2020). Functionally, like Nopp140, treacle also participates in rRNA transcription and processing (Nakhoul et al., 2014). More precisely, both treacle and Nopp140 seem to play similar roles in chaperoning snoRNPs to specific locations in the nucleoli (Baral et al., 2020). Also like Nopp140, treacle appears to be associated with the process of methylation of pre-rRNA as well as interactions with RNA Pol I (He et al., 2015).

Furthermore, there seems to be similarities in the way in which these gene disruptions present phenotypically. While TCS individuals display characteristic phenotypes, there is an interesting variability in its expression. There is a fairly broad spectrum of phenotypic expression among individuals with TCS – even among members of the same family. A clinical report from 1995 describes a woman with mild TCS who gave birth to a daughter displaying a more severe TCS phenotype (Fig. 2) (Hansen et al., 1996). It was shown that the child had no other interacting conditions, yet she displayed more severe craniofacial malformations and more life-threatening problems than her mother (Hansen et al., 1996). The variability of neural crest cell effects and phenotypic expression observed by the loss of treacle in individuals with TCS resembles the variability of phenotypic expression in different NB lineages displayed in *D. melanogaster* with the loss of Nopp140 (Baral et al., 2020).

Figure 2. Variability in the Treacher Collins Syndrome (TCS) phenotype. TCS individuals may display a wide range of physiological abnormalities. This image highlights the phenotypic differences between mother and daughter.

rRNA synthesis:

Ribosome production begins in the nucleolus of the cell, and the process of synthesis, exportation, and movement of these ribosomes is a series of many specific, ordered steps (Cooper, 2000). Ribosome synthesis begins with the synthesis of rRNA, which ultimately determines the cell's capacity for growth and proliferation (Grummt, 2013). While other types of RNA (mRNA, tRNA) are made in the nucleus, rRNA is made specifically in the nucleolus (Cooper, 2000).

In the nucleolus, RNA polymerase I (Pol I) synthesizes pre-ribosomal RNA from rDNA (He et al., 2015). The pre-RNA is then chemically modified with the help of small nucleolar RNAs (snoRNPs), specifically box C/D snoRNPs that guide methyltransferases for site specific 2'-O-methylation and box H/ACA snoRNPs that are responsible for site-specific pseudo-uridylation (He et al., 2015). Endo- and exo-nucleolytic cleavage of the modified pre-RNA then produces the mature 18S rRNA, which helps form the small ribosomal subunit, and the mature 5.8S and 28S rRNAs which ultimately form the large ribosomal subunit (He et al., 2015).

Goal of Study:

The goal of my research is to determine if the loss of the *Nopp140* gene affects rRNA synthesis in the nucleolus. Knowing how this gene deletion affects rRNA production allows a better understanding of the role the Nopp140 ribosome assembly factor plays in ribosome production. Looking at the larval brains and neuroblasts may also help elucidate the underlying mechanisms of stem cell/progenitor cell specificity observed in human ribosomopathies. As a model for human ribosomopathies, knowing this relationship between the *Nopp140* gene and ribosome synthesis can hopefully one day help identify both the exact cause of diseases like Treacher Collins and the extent to which they may develop.

Materials and Methods

Model Organism:

The model organism used in this study is *Drosophila melanogaster,* which has undergone nucleolar stress induced by CRISPR technology. Specifically, these *Drosophila* experienced a knockout of the *Nopp140* gene induced by the Baral et al. group (2020). The knockout larvae served as the experimental group and were contrasted with a control group, which was heterozygous for the *Nopp140* gene disruption over the wild type allele.

Flies used in this experiment were obtained from a stock manufactured by Baral, Lieux, and DiMario. To achieve the disruption of the *Nopp140* gene, CRISPR-mediated homology directed repair (HDR) was employed (Baral et al., 2020). A plasmid cocktail – a combination of two gRNA plasmids and *DsRed-Donor* plasmid – was injected into embryos homozygous for a Cas9 transgenic fly line, *nanos*-Cas9 (Baral et al., 2020). More specifically, the gRNAs directed a CRISPR-Cas9 deletion of a sequence of 321 bps within the second exon of the *Nopp140* gene, while HDR inserted the *DsRed* gene in its place (Baral et al., 2020). *DsRed* expresses itself under the *3xP3* eye promoter, which is active in both the embryonic and larval brain and the adult eyes, and therefore, makes the eyes fluoresce red in color (Baral et al., 2020). Thus, *DsRed* acted as a selectable marker, and *Nopp140* disruption events were confirmed visually by a *DsRed* positive phenotype (Baral et al., 2020).

Each of the seven confirmed *Nopp140* disrupted lines was maintained using a balancer chromosome, *TM3-GFP* (Baral et al., 2020). (The $J11^{DsRed}$ disrupted line was used for further experimentation.) This GFP reporter gene within the balancer chromosome fluoresces green in the heterozygote ($J11^{DsRed}/TM3\text{-}GFP$) larval gut tissue so that it may be visually distinguishable under blue light.

However, in order to visualize *Drosophila* brain tissue under multi-channel immunofluorescence and avoid interference in the red channel, CRISPR-Cas9 with non-homologous end joining (NHEJ) was then used to disrupt the *DsRed* gene within the $J11^{DsRed}$ allele (Baral et al., 2020). To achieve this disruption, two gRNA plasmids and a Cas9 vector were injected into $J11^{DsRed}/TM3$ embryos in order to mutate the *DsRed* gene in the second exon (Baral et al., 2020). The disruption was confirmed by RT-PCR analyses (Baral et al., 2020).

Fly Stock:

The two lines of *Drosophila melanogaster* used were taken from a J11/TM3-GFP stock, which when crossed, produce J11/TM3 and J11/J11 lines (and TM3/TM3 are inviable). As a result, the control group used was J11/TM3 which is *Nopp140* +/- and thus, displays GFP in the gut. The experimental group was the knockout line, J11/J11, which is *Nopp140* -/-.

Larvae Selection:

To obtain *D. melanogaster* larvae for both the experimental and control groups, flies from the J11/TM3-GFP stock were transferred to cages with grape juice agar plates with yeast as a food source. The grape juice agar plates were prepared from a mixture of grape juice, sugar, and Nipagin-M (a mold inhibitor), water, and agar. Plates were exchanged about every 3 days to maintain the stock and to collect larvae for experimental use.

To separate the experimental, knockout larvae (J11/J11) from the heterozygous, control larvae (J11/TM3), the agar plate of larvae was exposed to blue excitation light. The heterozygotes contained GFP in the gut and thus, were identifiable by green fluorescence under the blue light.

Conversely, the homozygote knockout larvae were identified by their non-fluorescence in the gut tissue.

BrUTP labeling:

To observe rRNA synthesis, BrUTP (5-Bromouridine 5'-triphosphate), a modified ribonucleotide, was used to label RNA *in vivo*. When live tissue is incubated with BrUTP, the ribonucleotide can be incorporated into nascent RNA. Then with primary antibody (anti-BrdU) and secondary antibody (Alexa-Fluor) labeling, the newly produced RNA can be visualized via fluorescence microscopy.

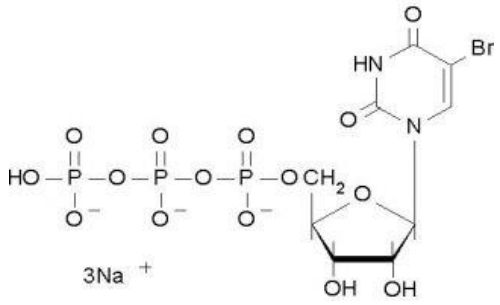

Figure 3. BrUTP structure. BrUTP is a nucleotide analog of uridine, which can be incorporated into RNA transcription. By modifying the structure of uridine with bromine, it can then be targeted with a primary antibody and then a secondary antibody so that it may be visualized.

To make the dissection buffer, 1.2 ml of 250 mM HEPES, 1.6 ml of 1 M KCl, 0.32 ml of 1 M NaCl, 0.1 ml of 1 M $MgCl_2$, 2 ml of 10% PEG 6000, and 14.78 ml of MilliQ water were added to a test tube. This solution was then set to a pH around 6.9-7.2.

For each of the two groups, two identical mixtures were then made. 225 µL of the

dissection buffer were gently mixed with 25 µL of FuGene 6 transfection reagent and left to stand for 5 minutes at RT. After 5 minutes, 27.5 µL of 100 mM BrUTP* were added to the 250 µL of the dissection buffer/FuGene 6 solution. This solution was left to stand for 15 minutes at RT to allow for the FuGene 6 to form a micelle around BrUTP. The FuGene 6 is a non-liposomal transfection reagent that has the capacity to carry BrUTP into the cell.

**100 mM BrUTP was prepared by adding 0.178 ml of MilliQ water to 10 mg of BrUTP.*

During this time, about ten larvae from the control group and ten larvae from the experimental group were placed into two separate wells and were submerged in dissection buffer. Towards the end of the 15 minutes, all larvae were dissected while in the buffer. For maximum efficiency, each larva was transferred into a new well (1 well for control group, 1 well for experimental group) containing the FuGene 6/BrUTP solution immediately after being dissected. The tissues were then left to incubate at RT for 30 minutes with shaking. Wells containing the tissues were placed in a petri dish on a moistened paper towel to prevent drying out.

After, the FuGene 6/BrUTP solution was removed and fresh dissection buffer was added for a 15-minute chase with shaking. During the chase, a fixing solution was made containing 1.85 ml of fresh 10% paraformaldehyde*, 2.5 ml of Acetic acid, and 0.65 ml of MilliQ water. After the 15-minute chase, the tissues were fixed for 10 minutes in the fixing solution.

**10% paraformaldehyde was prepared by adding 1 g of PFA to a total of 10 ml H_2O and 1 drop of 1 M NaOH.*

The following is according to Spradling's procedure for antibody labeling (De Cuevas & Spradling, 1996). After the tissues were fixed, they were washed with 1xPBS; 0.1% TX-100 with 0.04% azide two times over the course of 30 minutes. Next, the tissues were blocked with 3%

BSA in 1xPBS; 0.1% TX-100 with 0.04% azide for 30 minutes.

The tissues were then probed with a 1/250 dilution using 2 µL of the primary antibody, Rat anti-BrdU, in 500 µL of 3% BSA in 1xPBS; 0.1% TX-100 with 0.04% azide. So, 250 µL of this dilution were placed into each of the two wells, and the tissues were incubated at 4˚C overnight with gentle shaking.

The following day, the primary antibody was removed, and the tissues were washed with 1xPBS; 0.1% TX-100 with 0.04% azide for 1 hour with gentle shaking, washing every 10 minutes. This was followed by a 30-minute wash in 3% BSA in 1xPBS; 0.1% TX-100 with 0.04% azide.

The tissues were then incubated for 1 hour in a 1/400 dilution of the secondary antibody, which is the goat-anti rat Alexa Fluor-488 (green channel) antibody. The dilution was composed of 2 µL of the secondary antibody and 800 µL of 3% BSA in 1xPBS; 0.1% TX-100 with 0.04% azide.

After the hour, the tissues were washed three times with 1xPBS; 0.1% TX-100 with 0.04% azide followed by a 5-minute wash in DAPI (0.5 µL of DAPI in 1 mL 1xPBS; 0.1% TX-100 with 0.04% azide). Then, the tissues were left in the 1xPBS; 0.1% TX-100 with 0.04% azide to be further dissected and prepped for the microscope slide for visualization.

Fluorescence Microscopy:

Fluorescence microscopy aids in the observation of cell physiology by imaging fluorescent molecules (Sanderson et al., 2014). A laser acts as the light source and allows visualization of auto-fluorescence or expression of proteins using fluorescent antibodies, a technique termed immunofluorescence (Massachusetts Institute of Technology, 2015). There is a variety of

fluorescent indicators designed to target specific molecules, such as proteins or ions, so that the desired target may be excitable by light and therefore, visualized fluorescently (Sanderson et al., 2014).

From the light source, the laser travels through a filter cube, which uses one of the many color channels in order to emit the correct wavelength needed to excite the fluorescent molecules in the specimen (Massachusetts Institute of Technology, 2015). After hitting the sample, the fluorescent light is then reflected back through the objective and filter cube, which can then pass through either the eyepiece or camera (Massachusetts Institute of Technology, 2015).

This study, specifically, used indirect immunofluorescence. With this method, a primary antibody is applied first and is followed by a fluorescently tagged secondary antibody (Massachusetts Institute of Technology, 2015). The fluorescence may then be visualized by a specific coordinating wavelength controlled by the filter cube (Massachusetts Institute of Technology, 2015).

This study uses the green channel to capture fluorescence of the Alexa Fluor-488 secondary antibody used. Therefore, the green channel visualized the tagged rRNA in the nucleoli as well as RNA dispersed throughout the nucleus. This study also uses DAPI, which binds DNA and labels the nuclei. However, DAPI does not label the nucleolus being that it is the site of rRNA production, so the DAPI label essentially leaves a hole in the nuclei where the nucleoli occur. Since this study focuses on the nucleoli, both the DAPI channel and green channel can be used to determine the location of the nucleoli both through labeling and lack of labeling.

ImageJ analysis:

ImageJ is a software program designed for image processing and analysis. The program allows digital editing, magnification, and enhancement of images as well as quantifiable analysis, such as defining area and brightness scale values.

Using the ImageJ software, image overlay can be manipulated to create single images combining DAPI channel and green channel images. More precisely, this will overlap the labeled nucleoli in the green channel with the lack of nucleoli labeling in the DAPI channel. Thus, using this overlay technique, a rough outline of individual nucleoli can be made.

ImageJ automatically determines brightness values by converting the image to an 8-bit grayscale, which linearly scales brightness values on a scale of 0-255. The minimum, maximum, and mean values of brightness were recorded for each area outlined. Using this data, the mean brightness value of the nucleoli was divided by its area. This value serves as an indirect measure of the amount of rRNA transcribed in order to compare rRNA synthesis of the homozygote knockouts to the heterozygotes. This value may also help indirectly identify issues with ribosome production efficiency. Nucleoli for all images were outlined three times each for greater precision.

Results

BrUTP Labeling:

BrUTP successfully labeled all tissue types in both the *Nopp140-/+* and *Nopp140-/-* groups. This was confirmed using fluorescence microscopy visualization of multiple tissue samples. Images taken in the green channel revealed concentrated regions of rRNA synthesis in the nucleolar regions as well as individually transcribed genes interspersed throughout nuclei, which can be seen in Figure 4. Some images displayed clearly defined nucleoli and surrounding cell space while others were less defined.

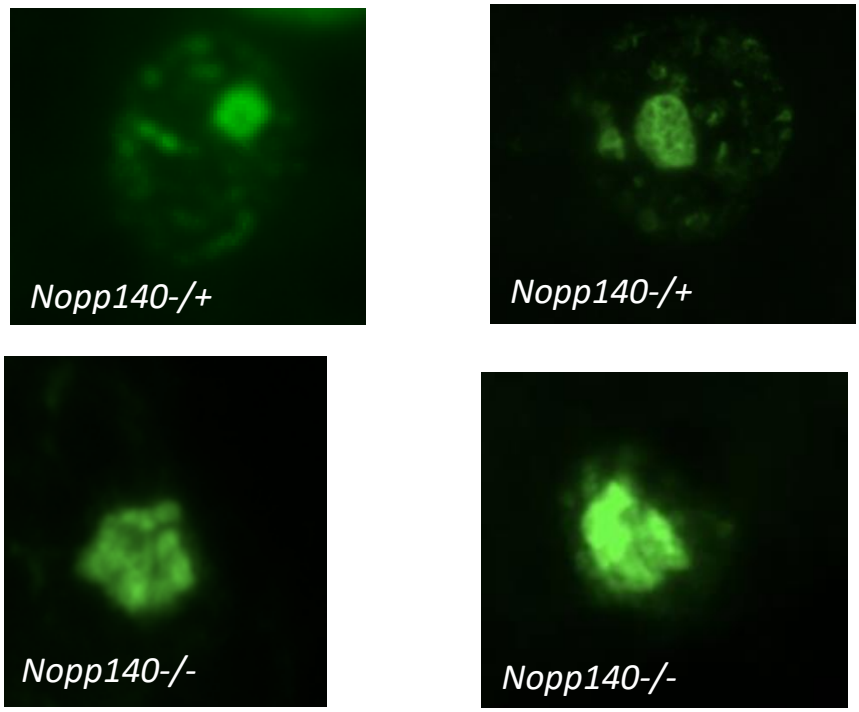

Figure 4. Green channel. Examples of well labeled RNA in both *Nopp140-/+* and *Nopp140-/-* larvae. The circles of concentrated labeling show rRNA in the nucleoli while the smaller areas of labeling indicate the newly transcribed RNA throughout the nucleus.

Additionally, the DAPI stain was visualized in the DAPI channel. This channel showed the labeled nuclei in blue but did not label the nucleoli, leaving a dark hole inside the labeled area. Again, some images were more defined than others.

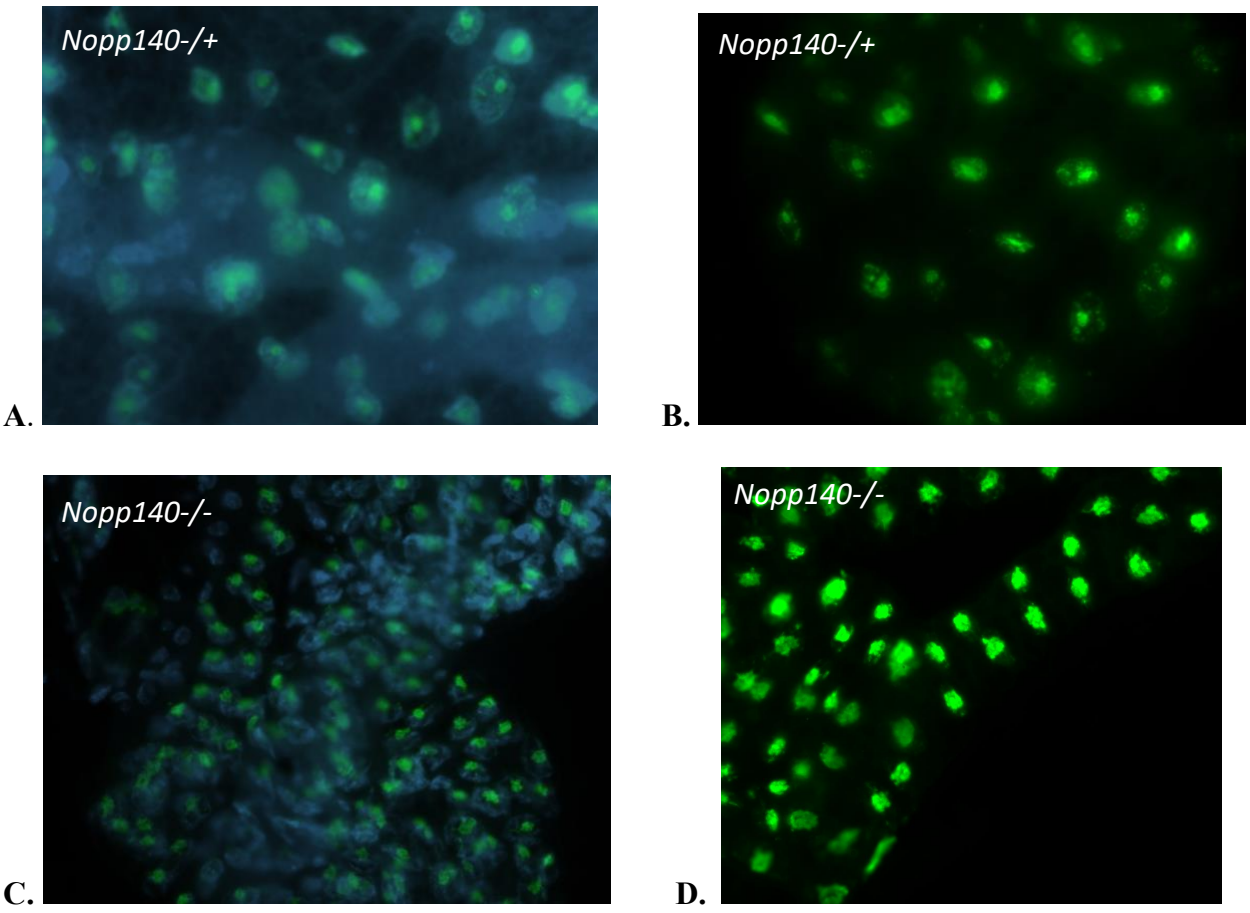

Figure 5. Overlay of fluorescence microscopy DAPI and green channels. The green channel shows labeled RNA in both the nucleoli, which sits in the unlabeled DAPI image, as well as in genes transcribed in the nucleus. **A.** 50% opacity overlay image of the heterozygous tissue (J11/TM3). **B.** Example of BrUTP labeling of J11/TM3 larval tissues in the green channel. **C.** 50% opacity overlay image of the homozygous knockout tissue (J11/J11). **D.** Example of BrUTP labeling of J11/J11 larval tissues in the green channel.

Neuroblasts:

While the brain lobes did show labeling in both the green and DAPI channels, there was variability in green channel labeling across J11/J11 samples. The ventral nerve cords appeared to label fairly consistently, but variability was seen in BrUTP labeling of the brain lobes.

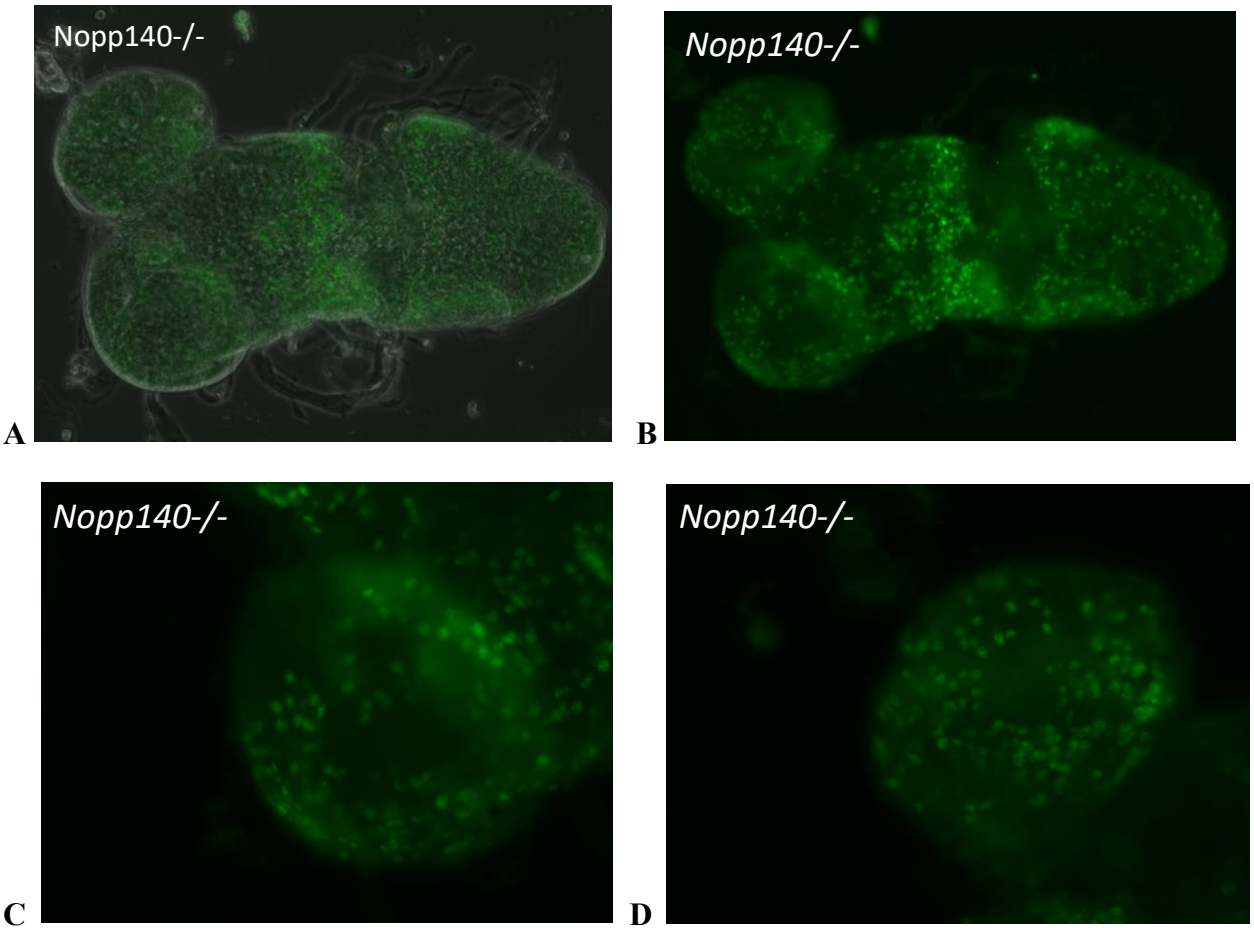

Figure 6. J11/J11 brain lobes and ventral nerve cord. 11-day old J11/J11 knockout larval brain imaging with strong labeling. **A.** Larval brain image using overlay of regular electron microscope image (no channel) and green channel at 50% opacity. **B.** Image of the full larval brain, including the ventral nerve cord and two brain lobes, in the green channel. **C.** Green channel image of one brain lobe shows strong labeling. **D.** Green channel image of the other brain lobe also shows strong labeling.

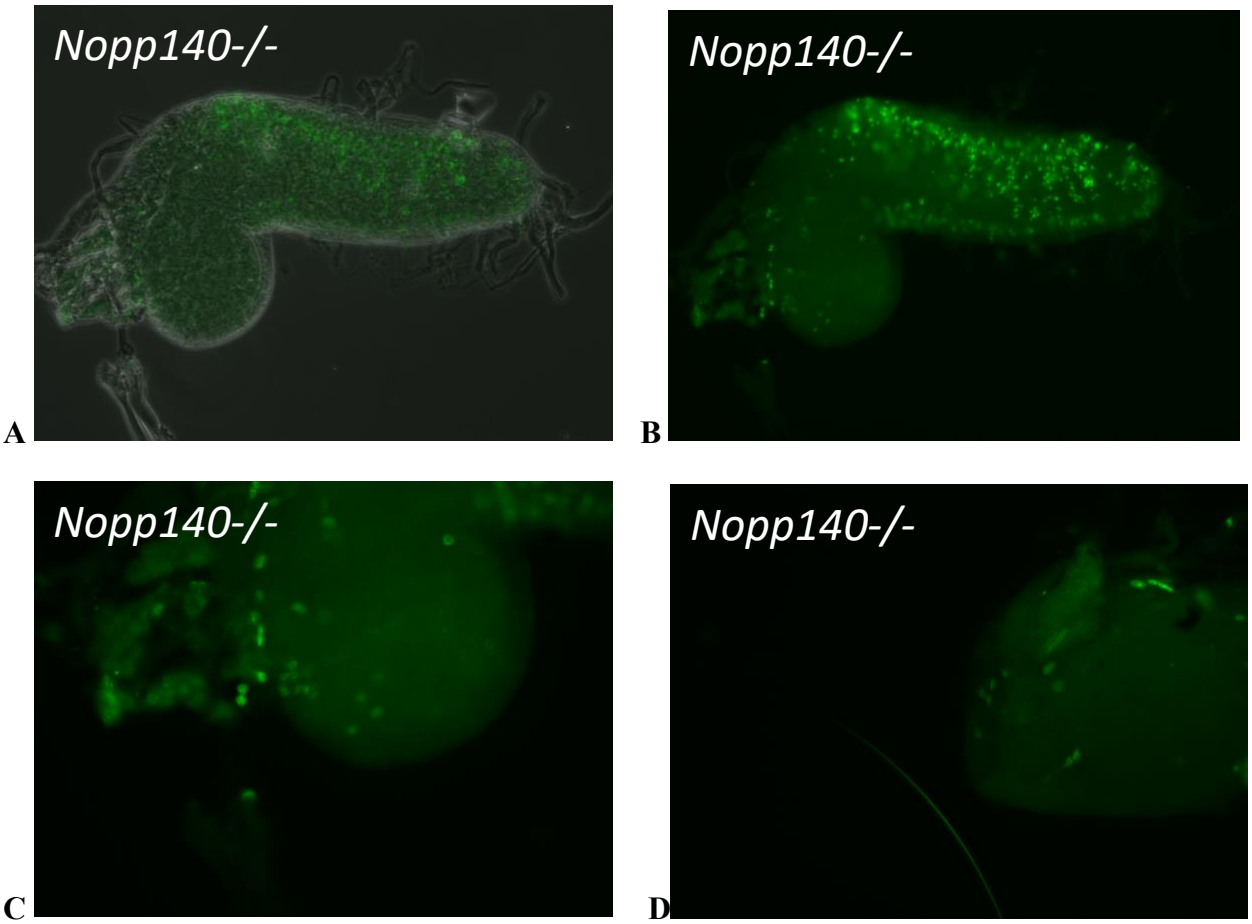

Figure 7. J11/J11 brain lobes and ventral nerve cord. 11-day old J11/J11 knockout larval brain imaging with partial labeling. **A.** Larval brain image using overlay of regular electron microscope image (no channel) and green channel at 50% opacity. **B.** Image of the full larval brain, including the ventral nerve cord and two overlapping brain lobes, in the green channel. **C.** Green channel image of one brain lobe shows poor labeling. **D.** Green channel image of the other brain lobe also shows poor labeling.

A

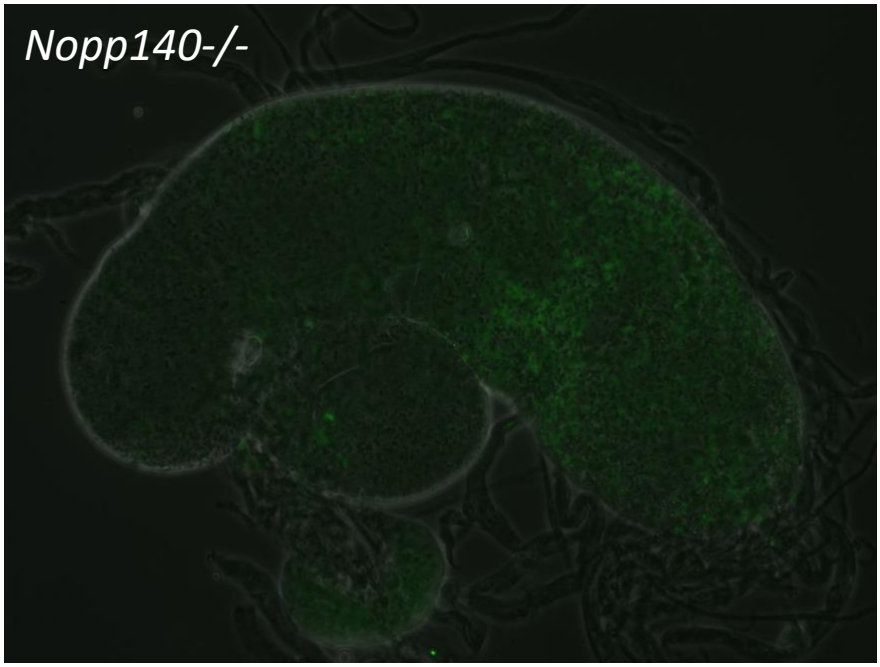

B

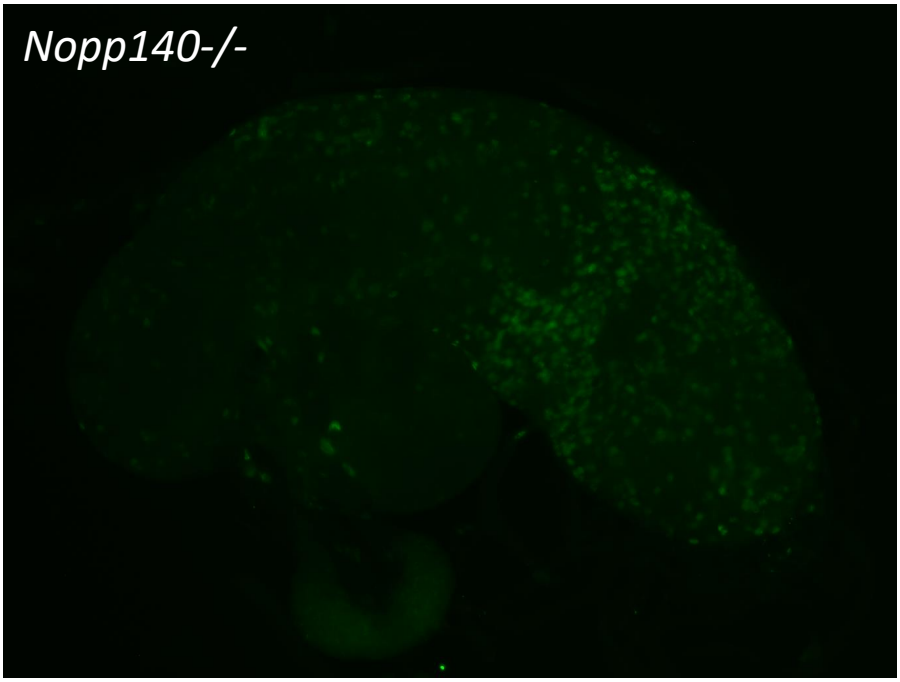

Figure 8. J11/J11 brain lobes and ventral nerve cord. Another 11-day old J11/J11 brain sample displaying partial labeling: good labeling on the ventral nerve cord and little to no labeling of brain lobes. **A.** Overlay of regular electron microscope image (no channel) and green channel at 70% opacity. **B.** Full larval brain, including the ventral nerve cord and two brain lobes, in the green channel.

Quantification of nucleolar fluorescence levels:

For the *Nopp140-/-* (J11/J11) larvae, mean brightness/area was calculated for individual nucleoli and was then averaged, resulting in a value of 0.3093 (n=3). The same calculation was performed for the *Nopp140-/+* larvae (J11/TM3), resulting in a mean value of 0.331 (n=3).

Discussion

BrUTP labeling:

Both the knockout J11/J11 and control J11/TM3 larvae seemed to label all tissues (e.g. gut tissue, fat body tissue, Malpighian tubules, etc.) consistently. Because some nucleoli appeared less defined however, some labeled areas were not included in calculations. The overlay technique was able to remedy this issue but only to an extent.

Neuroblasts:

While it is not yet fully understood, it is interesting to note that there was variability in labeling of the J11/J11 brain lobes specifically. The ventral nerve cords seemed to label well and consistently, whereas the brain lobes showed poor to good labeling in different larval samples. Figure 6 shows strong labeling throughout the *Nopp140-/-* brain, in both the brain lobes and ventral nerve cord while Figures 7 and 8 show poor labeling in the *Nopp140-/-* brain lobes but still fairly good labeling in the ventral nerve cords.

It may also be important to point out that Figures 6, 7, and 8 come from knockout larvae that were 11 days old. This is fairly old for these mutant larvae considering over half are expected to die at just 6 days old (Baral et al., 2020). Differential expression of ribosome biogenesis factors in stem/progenitor cells in the neural crest is thought to explain why some *Nopp140-/-* larvae display differences in survivorship – the reason over half of these larvae will die after just 6 days ALH while others can last until up to 24 days ALH (Baral et al., 2020). Baral et al. suggests that this difference in expression and in survival could be due to differences in the amount of maternal Nopp140 mRNA and/or protein inherited, but this is still something that requires further research (2020).

This variability in Nopp140-disrupted larvae seems to parallel the variability seen in TCOF1-disrupted human individuals. Perhaps, the variability in brain labeling could be related to the mechanism that causes the puzzling variability of expression in TCS individuals that was described in the Hansen et al. study in 1996.

Quantification of nucleolar fluorescence levels:

It is important to note that the precision in defining the nucleoli is not optimal. The nucleolus is not surrounded by a membrane but rather is organized around chromosomal regions, so its boundaries are not so distinct (Cooper, 2000). Therefore, only well-defined nucleoli were used in calculations. The overlay technique seems to be the best option in validating the true nucleoli, but hopefully, future studies may be able to more accurately define borders.

Comparing the brightness/area values, the J11/J11 knockout larvae had a value of 0.3093, and the J11/TM3 larvae had a value of 0.331. A higher value would indicate more rRNA synthesis. While the control group had a higher average, there does not seem to be a significant difference between the two. Looking at both the images and the mathematical calculations, the difference does not seem huge. Still, it important to note the accuracy of the tools used and hopefully, future studies may be able to expound upon and enhance the accuracy of these measurements to better quantify rRNA synthesis.

However, because there was not a large difference among these calculations, it must be considered that the process of rRNA synthesis is not the root cause of the ribosomopathy. Future studies will need to be conducted to further investigate the consequences of a *Nopp140* gene disruption. Nopp140 as a RBF carries out an array of functions that must also be considered and explored.

Future improvements on this study may involve shortening and/or varying the BrUTP pulse time, i.e. the amount of time BrUTP has to be incorporated into tissues. Future studies may also include HPG protein assays; this would go a step beyond RNA production. Similar to the process of BrUTP labeling, the HPG assay utilizes an analog of methionine to be incorporated into newly synthesized proteins *in vivo*. Future studies could also investigate the methylation process believed to be associated with Nopp140. In summary, these potential research opportunities would study ribosomal protein composition and modifications, both of which could aid in our understanding of ribosomopathies.

To conclude, the exact effects of the *Nopp140* gene disruption are still not fully known. Future studies must still be conducted to elucidate the roles of Nopp140, the consequences of its loss, and its link to ribosomopathies.

References

Baral, S. S., Lieux, M. E., & DiMario, P. J. (2020). Nucleolar stress in *Drosophila* neuroblasts, a model for human ribosomopathies. *Biology open*, *9*(4), bio046565. https://doi.org/10.1242/bio.046565

Chen, H. K., Pai, C. Y., Huang, J. Y., & Yeh, N. H. (1999). Human Nopp140, which interacts with RNA polymerase I: implications for rRNA gene transcription and nucleolar structural organization. *Molecular and cellular biology*, *19*(12), 8536-8546.

Cooper G. M. *The Cell: A Molecular Approach*. 2nd edition. Sunderland (MA): Sinauer Associates; 2000. "The Nucleolus". Available from: https://www.ncbi.nlm.nih.gov/books/NBK9939/

Cui, Z., & DiMario, P. J. (2007). RNAi knockdown of Nopp140 induces Minute-like phenotypes in Drosophila. *Molecular biology of the cell*, *18*(6), 2179–2191. https://doi.org/10.1091/mbc.e07-01-0074

De Cuevas, M., Lee, J. K., & Spradling, A. C. (1996). alpha-spectrin is required for germline cell division and differentiation in the Drosophila ovary. *Development*, *122*(12), 3959-3968.

Grummt, I. (2013). The nucleolus—guardian of cellular homeostasis and genome integrity. *Chromosoma*, *122*(6), 487-497.

Hansen, M., Lucarelli, M. J., Whiteman, D. A., & Mulliken, J. B. (1996). Treacher Collins syndrome: phenotypic variability in a family including an infant with arhinia and uveal colobomas. *American journal of medical genetics*, *61*(1), 71-74.

He, F., James, A., Raje, H., Ghaffari, H., & DiMario, P. (2015). Deletion of Drosophila Nopp140 induces subcellular ribosomopathies. *Chromosoma*, *124*(2), 191-208.

Massachusetts Institute of Technology (2015). Fluorescence Microscopy Animation. *StarCellBio*. star.mit.edu/CellBio/animations/index.html

Nakhoul, H., Ke, J., Zhou, X., Liao, W., Zeng, S. X., & Lu, H. (2014). Ribosomopathies: mechanisms of disease. *Clinical Medicine Insights: Blood Disorders*, *7*, CMBD-S16952.

Narla, A., & Ebert, B. L. (2010). Ribosomopathies: human disorders of ribosome dysfunction. *Blood, The Journal of the American Society of Hematology*, *115*(16), 3196-3205.

Sanderson, M. J., Smith, I., Parker, I., & Bootman, M. D. (2014). Fluorescence microscopy. *Cold Spring Harbor protocols*, *2014*(10), pdb.top071795. https://doi.org/10.1101/pdb.top071795

Sm. “5-Bromouridine 5′-Triphosphate Sodium Salt: CAS 161848-60-8.” *Santa Cruz Biotechnology*, Santa Cruz Biotechnology, Inc, 10 May 2015, www.scbt.com/p/5-bromouridine-5prime-triphosphate-sodium-salt-161848-60-8.